Mapping Electron Beam Injected Trapped Charge with Scattering Scanning Near-field Optical Microscopy

DENIS E. TRANCA,[1] EMILIO SÁNCHEZ-ORTIGA,[2] GENARO SAAVEDRA,[2] MANUEL MARTÍNEZ-CORRAL,[2] SYED A. M. TOFAIL,[3] STEFAN G. STANCIU,[1] RADU HRISTU,[1] GEORGE A. STANCIU[1,*]

[1] *Center for Microscopy - Microanalysis and Information Processing, University Politehnica of Bucharest. Bucharest, RO-060042, Romania*
[2] *3D Imaging and Display Laboratory, Department of Optics, University of Valencia, Valencia, 46100, Spain*
[3] *Department of Physics and Energy, and Materials and Surface Science Institute, University of Limerick, Limerick, Ireland*
**Corresponding author: stanciu@physics.pub.ro*

Received XX Month XXXX; revisedXX Month, XXXX; accepted XX MonthXXXX; posted XX Month XXXX (Doc. ID XXXXX); published XX Month XXXX

Scattering scanning near-field optical microscopy (s-SNOM) has been demonstrated as a valuable tool for mapping the optical and optoelectronic properties of materials with nanoscale resolution. Here we report experimental evidence that trapped electric charges injected by electron beam at the surface of dielectric samples affect the sample-dipole interaction, which has direct impact towards the s-SNOM image content. Nanoscale mapping of surface trapped charge holds significant potential for the precise tailoring of the electrostatic properties of dielectric and semi-conductive samples, such as hydroxyapatite, which has particular importance with respect to biomedical applications. The methodology developed here is highly relevant to semiconductor device fabrication as well.

OCIS codes: *(180.4243) Near-field microscopy; (160.1435) Biomaterials; (090.1995) Digital holography; (120.6650) Surface measurements, figure.*

http://dx.doi.org/10.1364/OL.99.099999

Scattering Scanning Near-field Optical Microscopy (s-SNOM) has been demonstrated in the past years as an extremely effective tool for imaging and mapping the surface properties of materials in the nanoscale. The complex contrast mechanisms of s-SNOM have enabled a wide range of applications such as electric permittivity mapping [1, 2], infrared spectroscopy measurements [3-5], and plasmonic response investigations [6, 7] with resolution beyond the diffraction limit [8, 9]. The functionality of this microscopy tool is based on local interactions between the tip of a nano-probe that is scanned across the sample surface and the molecules on the sample surface in the presence of an incident laser beam focused on the tip. The electric field component of the incident laser beam creates in the tip an oscillating electric dipole which emits light with the same wavelength as the incident beam [10, 11]. When the tip is in close proximity to the surface of a sample (on distances much shorter than the wavelength), the light emitted by the electric dipole is influenced (in terms of amplitude and phase of the electric field component) by the local dielectric function of the sample. Detecting the light emitted by the oscillating electric dipole requires higher-harmonic demodulation and interferometric detection techniques to suppress the background light (mainly composed by direct or multiple reflections from the probe and sample) and to facilitate the reconstruction of the near-field optical signal amplitude and phase.

Our experiment brings evidence that trapped charges (e.g. injected by an electron beam or an ion beam, both of which are common in semiconductor device processing and biomaterials sterilization) influence the oscillating dipole from the tip and thus directly impact the image contrast in s-SNOM. We exploit this phenomenon to use s-SNOM imaging for mapping trapped surface charge with nano-scale resolution.

The interaction between trapped electrical charges and an oscillating dipole in s-SNOM can be understood by recalling that the latter models the oscillations of plasma electrons from the metal tip. In the first half-cycle of the external oscillating electric field (Fig. 1a) the field points to the tip from the sample. The plasma electrons in the tip are then directed towards the sample. In the case when no trapped charge is present on the surface, we assume that at the maximum elongation of the dipole an electric field of amplitude E_o is generated at the tip. Conversely, when a trapped charge is present at the surface in the proximity of the tip, a repulsive electric force occurs between the trapped charge and the plasma electrons at the tip-material surface interface. As a result, the elongation of the plasma electrons' oscillation decreases, which results in a decrease ΔE of the amplitude of the generated electric field. In the second half-cycle of the incident electric field (Fig. 1b) the field is pointing from the tip to the sample. In this case, the plasma electrons from the tip are directed backwards from the sample. Trapped charges now cannot affect the plasma electrons because the electric field of the trapped charge is screened by the nuclei of the metal atoms.

Within this context, let us consider the emitted electric field intensity to have the simple form $E_o \sin(\omega t)$, where ω is the angular frequency and t is time, and integrate it over a period T. In the absence of any

trapped surface charge the light intensity will be proportional to the value $E_o^2/2$. Conversely, with trapped surface charges the emitted electric field intensity will be $(E_o - \Delta E)\cdot \sin(\omega t)$ in the first half-cycle and $E_o \sin(\omega t)$ in the second half cycle. The intensity of the emitted light will then be proportional to a reduced factor, $E_o^2/4 + (E_o - \Delta E)^2/4$. This inherent variation in the light intensity due to the presence of trapped surface charge can be detected with nanoscale resolution in an s-SNOM.

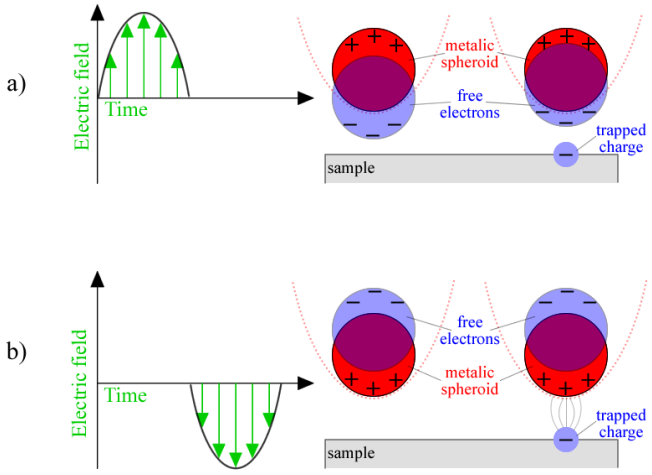

Fig. 1. Schematics of the localized surface plasmons excited by the oscillating electric field of an incident laser beam. The displacement of the plasma electrons (negative charge) relatively from the fixed lattice of atoms leaves a positive charge in the opposite direction; a) in the first half-cycle of the oscillating electric field, the plasma electrons from the tip are affected by the presence of the charge trapped on the surface of the sample; b) in the second half-cycle of the oscillating electric field, the trapped charge has no influence on the plasma electrons from the tip as the field is screened by the positive charge.

We test the above hypothesis in a practical setting on a hydroxyapatite (HA) thin film deposited on a silicon wafer by a spin-coating method. HA is one of the key biomaterials currently used for dental and orthopedic implants. Its dielectric properties and induced polarization have been investigated in the recent years because of the influence of electron beam injected trapped charge in stimulating specific protein binding through Coulumbic interactions [12, 13]. Details about the HA thin films fabrication procedure and about the ring-shaped negative charged areas can be found in previous publications [14-17]. Figure 2 shows atomic force microscopic images in cross-section. The thickness of the HA layer has been found to be approximately 560 nm. A 20 keV energy electron beam was used to irradiate the HA surface in a scanning electron microscope chamber at a pressure of 10^{-4} Pa. As a result, a trapping of charge at the location of surface defects takes place without any modification of the topography [14-17]. As it has been reported by these authors with the help of Kelvin Probe Force Microscopy (KPFM), phase AFM and photoluminescence (PL) measurements, the trapped charges injected from the electron beam lead to a negatively charged ring-shaped area on the surface.

In addition to the formation of a negative charged area on the HA surface, electron beam can cause dissociation of residual hydrocarbons [17] that can lead to carbon contaminations as it has been shown by AFM phase imaging [16].

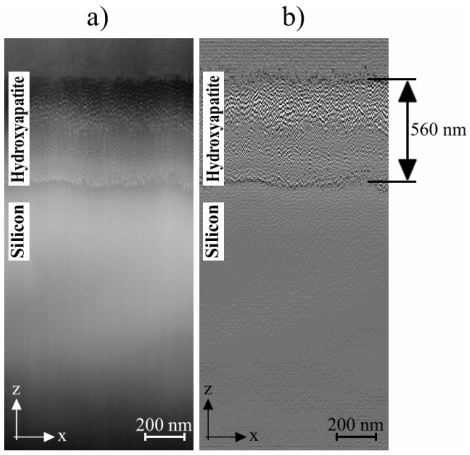

Fig. 2. AFM investigation in XZ plane to measure the thickness of the HA layer; a) topography; b) derivative of the topography image highlights better the dimension the HA layer.

The presence of the trapped charge caused photoluminescence which was imaged with diffraction-limited submicron range resolution using a laser scanning microscopy technique [16]. Here we successfully demonstrate direct imaging of these trapped charges with one order of magnitude higher resolution using s-SNOM. As the resolution in s-SNOM depends on the dimension of the scanning tip much higher resolutions can be achieved with tips with smaller radius of curvature.

s-SNOM investigations were conducted using a custom-made module working on a pseudo-heterodyne detection scheme [18, 19], which was implemented as an upgrade to a commercial Quesant Q-Scope 350 AFM. In such AFM based configurations simultaneous s-SNOM and AFM imaging is possible, as the oscillatory movement of the cantilever tip, specific to the AFM tapping workmode, enables as well higher harmonic demodulation for s-SNOM imaging. The light source used for the s-SNOM investigations was a semiconductor laser with a 638 nm wavelength and 0.1 mW power.

As a first step, simultaneous AFM and s-SNOM investigations have been performed. The AFM image (Fig. 3a) shows the absence of any topographic modification due to charge or carbon contamination. The AFM phase imaging (Fig. 3b), however, shows a disk shape corresponding to the carbon contamination [16]. The correspondence between the signals recorded by AFM phase imaging and carbon contamination has been previously discussed in [16]. The s-SNOM image (Fig. 3c) reveals a ring shaped structure which could be linked either to a change in the refractive index or to electric charge influence on the oscillating dipole, as hypothesized earlier.

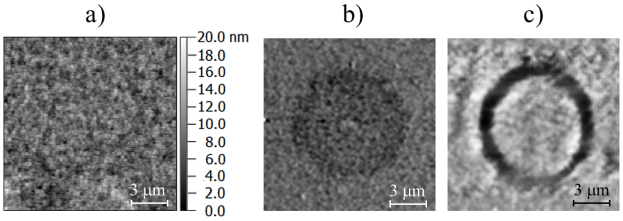

Fig. 3. AFM investigations on the HA sample; a) topography of the sample, revealing a flat surface; b) the same area investigated by AFM phase imaging, revealing a disk shape; c) s-SNOM image (second harmonic demodulation) of the same area, revealing a ring shaped structure.

For correctly assessing the influence of the trapped surface charge towards s-SNOM image formation, we have eliminated all possible influences that might lead to artifacts, which could bias the conclusions.

In a first step we assured that photoluminescence, topographic features and variations of the refractive index (due to the carbon contamination, for instance) didn't introduce artifacts in the s-SNOM images that we had collected.

Regarding the photoluminescence, it is known that hydroxyapaptite has a very large band-gap (3.95 eV) [20]. This means that it yields no pholuminescence for photon energy levels lower than the bandgap energy, which is the case of the visible range. However in same cases, the photoluminescence, having less energy than bandgap energy, was detected and it could be attributed to localized energy levels (deep or schallow levels within bandgap) [16, 20]. These levels might even correspond to stoichiometry deviations in the crystallyne lattice or might be radiation induced. Previously we reported a photoluminescence effect when the same samples were illuminateed by Ar:ion laser beam (488 nm) [16]. No photoluminescence was detected when samples were excited with 633 nm (He-Ne) wavelength radiation.

To verify if topography artifacts influenced in our case the content of the s-SNOM images, special attention was given to the scanning parameters and to the roughness of the sample's surface. The scanning parameters were carefully chosen so that the AFM high-precision feedback system together with a low scanning speed assured for the absence of error signal artifacts [21]. Moreover, roughness analysis reported the absence of sample features with step-like topography edges. This assures the absence of edge-darkening effects, another important topography-related artifact [21]. Indeed, the surface of the sample can be considered almost flat, which is confirmed by an average roughness (R_a) of 0.33 nm and a root mean square (RMS) of only 0.43 nm. To investigate the influence of the refractive index in the s-SNOM image, the HA surface was investigated by using Digital Holographic Microscopy (DHM); we have used a setup based on a Mach-Zehnder interferometer working in reflection mode [22, 23]. The light source was a He-Ne laser of wavelength of 633 nm and a beam-splitter was used for splitting the beam so as to produce the reference and the object waves. The holograms formed by the interference between the reference wave (a plane wave) and the object wave (reflected wave from the object) were captured with a CCD camera with 1024x1024 square pixels of 6.9 μm side. More details about the setup can be found in [24, 25]. DHM is capable of measuring the phase changes of the reflected light coming from the interface between HA and the underlying silicon dioxide layer. The differences of light phase are related to different optical path lengths in the sample and both geometric path and refractive index may influence the optical path. In our case the HA surface can be considered as flat as this has been shown by the performed AFM investigations. The surface of the silicon wafer is also flat and parallel to the HA surface. This ensured a constant geometric path along the surface of the sample. Thus, variations in light phase detected by DHM were generated only by variations of the refractive index. Note that the light phase images measured by DHM are only related to the optical path lengths and are essentially different from phase images acquired by tapping mode AFM, which gives information about phase variations in the oscillation of the AFM cantilever. Fig. 4 shows the DHM light phase image collected on a region where the charging procedure described earlier was applied.

Further on, we have calculated the average DHM wave phase difference for a total number of forty charged regions situated on the same HA sample, in order to determine the refractive index difference which occurs between the disk areas and the area which surrounds the disks. Using a custom MATLAB code, each individual disk region was enclosed in a square with an area double than the area of the disk. Forty sub-images were obtained this way, each containing a single disk and a background region of the same area. For each sub-image, an image mask was created to differentiate the area exposed to the electron beam from the unexposed area. The image masks were created employing an edge detection algorithm based on the Canny method [26]. Using these masks, we have calculated the mean phase values for the disk areas and for the background areas. This procedure revealed a mean phase difference of 0.6±0.2 radians between the areas exposed to the electron beam and the unexposed areas.

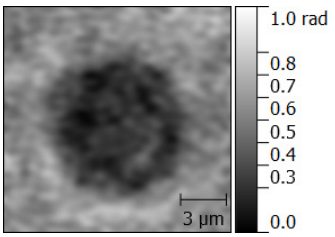

Fig. 4. Phase image of DHM investigation on the HA sample revealing a phase range between 0-1 radians.

Taking into account that the HA layer has a thickness of 560 nm and that the refractive index of HA is about 1.65 [27] for the areas unexposed to the electron beam, the refractive index of the areas exposed to the electron beam has been derived to have a value of 1.6±0.01. Thus, the index difference between the two regions is approximately 3%.

An important question to answer is, do such refractive index variations (3%) have a notable influence towards the recorded s-SNOM signals? For answering this question, we refer to our recent quantitative investigations regarding the dielectric function measurements with s-SNOM [28], which revealed a capability of measuring refractive index differences of more than 3.9% on SiO_2 and more than 5.7% on Si. Thus, a 3% index variation is indeed too small to be currently visualized by our s-SNOM system.

Summarizing, we demonstrated that the photoluminescence light does not influence the s-SNOM signal in our experiment. Furthermore, provided that the sample's surface is nearly flat and that it does not possess step-like topography edges, we conclude that the topography does not induce artifacts in the s-SNOM images. Moreover, the small change in refractive index (3%) revealed by DHM investigations and also the different shape (disk in DHM image, compared to ring shape in s-SNOM image) assure a negligible influence of the refractive index variation on the s-SNOM images. The absence of all these factors entitle us to conclude that the s-SNOM image collected in the frame of our experiment depict nothing else but the trapped charge that was injected by electron beam bombardment on the HA surface.

Our experiment thus shows for the first time that s-SNOM can be employed for measuring trapped surface charge in dielectrics and semiconductors with sub-diffraction resolution. This can be particularly useful in semiconductor devices where lithographic patterning through e-beam lithography and reactive ion etching may leave areas with trapped charges.

In conclusion, our experiments demonstrated that s-SNOM can be used to detect and map the surface trapped charge. This represents an important feature of s-SNOM systems especially for the cases when surface charge measurements with nano-resolution are needed. With more tools at hand for the assessment, characterization and tailoring of discrete electrostatic domains on biomaterials, such as hydroxyapatite, the scientific community will be able to expand the current understanding of the impact that surface charge holds over biological interactions between in-body elements and biomaterials. Such advancements are needed for developing novel surface charge patterning strategies that provide better integration of scaffolds and implants in the human body.

Acknowledgements. This work has received support from the European Community's Seventh Framework Programme (FP7/2012-

2015) under grant agreement no. 280804 (LANIR, www.lanir.eu) and no. 212533 (BioElectricSurface, www.bioelectricsurface.eu). This communication reflects the views only of the authors, and the Commission cannot be held responsible for any use which may be made of the information contained therein. The presented work has been supported as well by the Romanian Executive *Agency* for Higher Education, Research, Development and Innovation Funding through the research grants PN-II-PT-PCCA-2011-3.2-1162 (NANOLASCAN) and PN-II-RU-TE-2014-4-1803 (MICRONANO). The work of D.E.T. is supported by the Sectoral Operational Programme Human Resources Development (SOP HRD), financed from the European Social Fund and the Romanian Government under the contract number POSDRU/159/1.5/S/137390/. The authors acknowledge Dr. Maros Gregor and Professor Andrej Plecenick, Comenius University, Slovakia for providing hydroxyapatite thin films with electron-beam injected trapped charges.

References

1. A. A. Govyadinov, I. Amenabar, F. Huth, P. S. Carney, and R. Hillenbrand, J Phys Chem Lett **4**, 1526-1531 (2013).
2. A. A. Govyadinov, S. Mastel, F. Golmar, A. Chuvilin, R. S. Carney, and R. Hillenbrand, Acs Nano **8**, 6911-6921 (2014).
3. J. M. Stiegler, Y. Abate, A. Cvitkovic, Y. E. Romanyuk, A. J. Huber, S. R. Leone, and R. Hillenbrand, Acs Nano **5**, 6494-6499 (2011).
4. J. M. Hoffmann, B. Hauer, and T. Taubner, Appl Phys Lett **101,** 193105:1-4 (2012).
5. Z. Nuno, B. Hessler, B. Heiberg, R. Damato, T. Dunlap, Y. S. Shon, and Y. Abate, J Nanopart Res **14,** 1-8 (2012).
6. M. Schnell, A. Garcia-Etxarri, A. J. Huber, K. Crozier, J. Aizpurua, and R. Hillenbrand, Nat Photonics **3**, 287-291 (2009).
7. D. S. Kim, and Z. H. Kim, Opt Express **20**, 8689-8699 (2012).
8. A. Horneber, K. Braun, J. Rogalski, P. Leiderer, A. J. Meixner, and D. Zhang, Phys Chem Chem Phys **17**, 21288-21293 (2015).
9. T. W. Johnson, Z. J. Lapin, R. Beams, N. C. Lindquist, S. G. Rodrigo, L. Novotny, and S. H. Oh, Acs Nano **6**, 9168-9174 (2012).
10. B. Knoll, and F. Keilmann, Opt Commun **182**, 321-328 (2000).
11. A. Cvitkovic, N. Ocelic, and R. Hillenbrand, Opt Express **15**, 8550-8565 (2007).
12. S. Robin, A. A. Gandhi, M. Gregor, F. R. Laffir, T. Pecenik, A. Pecenik, T. Soulimane, and S. A. M. Tofail, Langmuir **27**, 14968-14974 (2011).
13. T. Plecenik, S. Robin, M. Gregor, M. Truchly, S. Lang, A. Gandhi, M. Zahoran, F. Laffir, T. Soulimane, M. Vargova, G. Plesch, P. Kus, A. Plecenik, and S. A. M. Tofail, J Mater Sci-Mater M **23**, 47-50 (2012).
14. T. Plecenik, S. A. M. Tofail, M. Gregor, M. Zahoran, M. Truchly, F. Laffir, T. Roch, P. Durina, M. Vargova, G. Plesch, P. Kus, and A. Plecenik, Appl Phys Lett **98,** 113701:1-3(2011).
15. R. Hristu, S. A. M. Tofail, S. G. Stanciu, D. E. Tranca, and G. A. Stanciu, Int C Trans Opt Netw (2014).
16. R. Hristu, D. E. Tranca, S. G. Stanciu, M. Gregor, T. Plecenik, M. Truchly, T. Roch, S. A. M. Tofail, and G. A. Stanciu, Microsc Microanal **20**, 586-595 (2014).
17. R. Hristu, S. G. Stanciu, D. E. Tranca, and G. A. Stanciu, Appl Surf Sci **346**, 342-347 (2015).
18. C. Stoichita, R. Hristu, S.G. Stanciu, G. Stanciu, 2009 3rd ICTON Mediterranean Winter Conference (ICTON-MW)2009.
19. N. Ocelic, A. Huber, and R. Hillenbrand, Appl Phys Lett **89,** 101124:1-3 (2006).
20. G. Rosenman, D. Aronov, L. Oster, J. Haddad, G. Mezinskis, I. Pavlovska, M. Chaikina, and A. Karlov, J Lumin **122**, 936-938 (2007).
21. *Nano-optics and near-field optical microscopy* (Artech House, 2009).
22. A. Doblas, E. Sanchez-Ortiga, M. Martinez-Corral, G. Saavedra, P. Andres, and J. Garcia-Sucerquia, Proc Spie **8785** (2013).
23. A. Doblas, E. Sanchez-Ortiga, M. Martinez-Corral, G. Saavedra, and J. Garcia-Sucerquia, J Biomed Opt **19,** 046022:1-8 (2014).
24. E. Sanchez-Ortiga, P. Ferraro, M. Martinez-Corral, G. Saavedra, and A. Doblas, J Opt Soc Am A **28**, 1410-1417 (2011).
25. E. Sanchez-Ortiga, A. Doblas, G. Saavedra, M. Martinez-Corral, and J. Garcia-Sucerquia, Appl Optics **53**, 2058-2066 (2014).
26. T. Sun, and C. Z. Gao, Appl Mech Mater **291-294**, 2869-2873 (2013).
27. *The biochemistry and physiology of bone* (Elsevier, 2014).
28. D. E. Tranca, S. G. Stanciu, R. Hristu, C. Stoichita, S. A. M. Tofail, and G. A. Stanciu, Scientific Reports **5,** 11876:1-9 (2015).

Full References

Govyadinov, A.A., et al., Quantitative Measurement of Local Infrared Absorption and Dielectric Function with Tip-Enhanced Near-Field Microscopy. Journal of Physical Chemistry Letters, 2013. **4**(9): p. 1526-1531.

Govyadinov, A.A., et al., Recovery of Permittivity and Depth from Near-Field Data as a Step toward Infrared Nanotomography. Acs Nano, 2014. **8**(7): p. 6911-6921.

Stiegler, J.M., et al., Nanoscale Infrared Absorption Spectroscopy of Individual Nanoparticles Enabled by Scattering-Type Near-Field Microscopy. Acs Nano, 2011. **5**(8): p. 6494-6499.

Hoffmann, J.M., B. Hauer, and T. Taubner, *Antenna-enhanced infrared near-field nanospectroscopy of a polymer.* Applied Physics Letters, 2012. **101**(19): p. 193105:1-4.

Nuno, Z., et al., Nanoscale near-field infrared spectroscopic imaging of silica-shell/gold-core and pure silica nanoparticles. Journal of Nanoparticle Research, 2012. **14**(3): 1-8.

Schnell, M., et al., Controlling the near-field oscillations of loaded plasmonic nanoantennas. Nature Photonics, 2009. **3**(5): p. 287-291.

Kim, D.S. and Z.H. Kim, Role of in-plane polarizability of the tip in scattering near-field microscopy of a plasmonic nanoparticle. Optics Express, 2012. **20**(8): p. 8689-8699.

Horneber, A., et al., *Nonlinear optical imaging of single plasmonic nanoparticles with 30 nm resolution.* Physical Chemistry Chemical Physics, 2015. **17**(33): p. 21288-21293.

Johnson, T.W., et al., Highly Reproducible Near-Field Optical Imaging with Sub-20-nm Resolution Based on Template-Stripped Gold Pyramids. Acs Nano, 2012. **6**(10): p. 9168-9174.

Knoll, B. and F. Keilmann, Enhanced dielectric contrast in scattering-type scanning near-field optical microscopy. Optics Communications, 2000. **182**(4-6): p. 321-328.

Cvitkovic, A., N. Ocelic, and R. Hillenbrand, Analytical model for quantitative prediction of material contrasts in scattering-type near-field optical microscopy. Optics Express, 2007. **15**(14): p. 8550-8565.

Robin, S., et al., Charge Specific Protein Placement at Submicrometer and Nanometer Scale by Direct Modification of Surface Potential by Electron Beam. Langmuir, 2011. **27**(24): p. 14968-14974.

Plecenik, T., et al., Directly created electrostatic micro-domains on hydroxyapatite: probing with a Kelvin Force probe and a protein. Journal of Materials Science-Materials in Medicine, 2012. **23**(1): p. 47-50.

Plecenik, T., et al., Direct creation of microdomains with positive and negative surface potential on hydroxyapatite coatings. Applied Physics Letters, 2011. **98**(11): p. 113701:1-3.

Hristu, R., et al., *Hydroxyapatite Surface Charge Investigated by Scanning Probe Microscopy.* 2014 16th International Conference on Transparent Optical Networks (Icton), 2014.

Hristu, R., et al., Surface Charge and Carbon Contamination on an Electron-Beam-Irradiated Hydroxyapatite Thin Film Investigated by Photoluminescence and Phase Imaging in Atomic Force Microscopy. Microscopy and Microanalysis, 2014. **20**(2): p. 586-595.

Hristu, R., et al., Electron beam influence on the carbon contamination of electron irradiated hydroxyapatite thin films. Applied Surface Science, 2015. **346**: p. 342-347.

C. Stoichita, R. Hristu, S.G. Stanciu, G. Stanciu, "Near field investigation based on a novel apertureless near field optical microscope," presented at the 2009 3rd ICTON Mediterranean Winter Conference (ICTON-MW) 2009.

Ocelic, N., A. Huber, and R. Hillenbrand, *Pseudoheterodyne detection for background-free near-field spectroscopy.* Applied Physics Letters, 2006. **89**(10): p. 101124:1-3.

Rosenman, Gil, et al. Photoluminescence and surface photovoltage spectroscopy studies of hydroxyapatite nano-bio-ceramics. *Journal of luminescence*, 2007, 122: 936-938.

Zayats, Anatoly V., and David Richards. *Nano-optics and near-field optical microscopy*. Artech House, 2009.

Doblas, A., et al., *Curvature phase factor in digital holographic microscopy.* 8th Iberoamerican Optics Meeting and 11th Latin American Meeting on Optics, Lasers, and Applications, 2013. **8785**.

Doblas, A., et al., Accurate single-shot quantitative phase imaging of biological specimens with telecentric digital holographic microscopy. Journal of Biomedical Optics, 2014. **19**(4): p. 046022:1-8.

Sanchez-Ortiga, E., et al., *Digital holographic microscopy with pure-optical spherical phase compensation.* Journal of the Optical Society of America a-Optics Image Science and Vision, 2011. **28**(7): p. 1410-1417.

Sanchez-Ortiga, E., et al., Off-axis digital holographic microscopy: practical design parameters for operating at diffraction limit. Applied Optics, 2014. **53**(10): p. 2058-2066.

Sun, T. and C.Z. Gao, *An improved Canny edge detection algorithm.* Advances in Energy Science and Technology, Pts 1-4, 2013. **291-294**: p. 2869-2873.

The biochemistry and physiology of bone. Editor: G. H. Bourne, 2014, New York: Elsevier.

Tranca, D. E., et al. High-resolution quantitative determination of dielectric function by using scattering scanning near-field optical microscopy. *Scientific reports*, 2015, 5: p. 11876:1-9.